

Incompressible SPH Simulation of Double-Diffusive Convection Phenomena

Masaya Shigeta,* Takahiro Watanabe, Seiichiro Izawa, and Yu Fukunishi

Department of Mechanical Systems and Design, Tohoku University

6-6-01 Aramaki-Aoba, Aoba-ku, Sendai, 980-8579, Japan

*Email: shigeta@fluid.mech.tohoku.ac.jp

Abstract

An incompressible SPH method was developed to simulate double-diffusive convection phenomena, including the simultaneous diffusions of temperature and salinity, and both two-dimensional and three-dimensional simulations were carried out. The “salt-finger phenomenon” resulting from instability at the interface between liquids with two different densities was successfully simulated. The results indicated that the ratio between the speed of temperature conduction and the salinity diffusion controlled the overall phenomenon. Additionally, the “Christmas-tree phenomenon” was successfully simulated. The results revealed that this phenomenon did not take place when the salinity profile had a vertically constant gradient, but only when the original salinity profile had a staircase-like profile with layers of several steps. Although the results indicated that the developed SPH method is capable of reproducing the basic features of the phenomena, a discrepancy in the growth rates remains.

1. INTRODUCTION

1.1 SPH method

The Smoothed Particle Hydrodynamics (SPH) method has been developed as a particle method and applied to various fields of science and engineering. Lucy [1] and Gingold [2] first proposed the SPH method to model astrophysical problems; however, it has also been used for analyses of the ultra-fast crash [3] and heat conduction [4]. Because the SPH method is a mesh-free technique described in Lagrangian form according to the Navier-Stokes equation, it has higher adaptability for problems with deformation of the flow field and complicated movement of the boundaries than the Eulerian method, the Finite-Difference Method (FDM), and the Finite-Element Method (FEM).

Although the SPH method was originally developed for the analyses of compressible flows, in recent years it has been used to analyze incompressible viscous flows [5-10]. Particularly with the density homogenization algorithm proposed from the state equation of density and pressure [8], excellent results have been reported for a thermal-conductive flow with phase change [9] and a free surface as well as a moving interface [10]. However, instability at the interfaces cannot be evaluated precisely in double-diffusive convection fields, including the simultaneous diffusion process of temperature and concentration.

1.2 Double-diffusive convection: Salt-finger and Christmas-tree phenomena

The density of salty water decreases with rising temperature, but increases with increased salinity. In salty water, heat conducts 100 times faster than the diffusion of the dissolved salt. As a result, the water reaches thermal equilibrium with its surroundings far sooner than it achieves chemical equilibrium by sharing dissolved salt. For example, in the ocean, because of surface evaporation caused by the Sun, warm salty water may lie on top of colder less-salty water. In such cases, because the warm salty water cools down before it loses salt, the salty water becomes denser than the cold less-salty water below; then narrow streams of salty water start to descend, further decreasing its temperature. However, pure water rises, increasing its temperature. Because this phenomenon occurs in scales of only a few centimeters, the slender streams formed by this process are known as “salt fingers.” Since the discovery of this double-diffusive convection [11], salt-

finger convection has been widely recognized as an important mechanism for mixing heat and salt both vertically and laterally in the ocean. Therefore, many experimental studies [12-16], theories [17, 18], and two-dimensional numerical simulations [19-22] have focused on salt-water convection. However, due to instability at the interface between the fluids, this phenomenon has not yet been evaluated by particle methods. It is also important to simulate and analyze this phenomenon three-dimensionally because its fluid motions are inherently three-dimensional.

Tsinober et al. [23] reported on another kind of double-diffusive convection, the “Christmas-tree phenomenon.” According to their study, when a point source of heat was placed in fluid with a stable vertical salinity gradient, horizontal stratiform convection was observed in addition to the normal vertical convection. Although a two-dimensional numerical simulation using a grid-based scheme for a similar phenomenon caused by an iceberg on the ocean has been conducted [24], neither a two-dimensional nor a three-dimensional Lagrangian approach has ever been attempted.

1.3 Objective

The objective of this study was to develop an incompressible SPH method that could precisely and effectively simulate flow fields with double-diffusive convection. The two kinds of double-diffusive convection phenomena mentioned above were simulated both two-dimensionally and three-dimensionally. In this study, the time evolutions of the internal fields (e.g., temperature, salinity, and density) were investigated in addition to the flow structures. Also, the conditions in which these two characteristic double-diffusive convections occurred were clarified.

2. COMPUTATIONAL METHOD

2.1 Basic idea

The SPH method is a gridless Lagrangian-based approach to solve problems of fluid dynamics, proposed by Lucy [1] and Gingold et al. [2]. In the SPH method, the fluid motion is represented by the behavior of particles with mass, velocity, and several additional fluid quantities. These quantities of one particle are distributed around the center of the particle by an interpolating kernel function, and the physical quantities at a certain position are expressed as the summation of them over the particles.

$$f(\mathbf{r}) = \sum_b f_b \frac{m_b}{\rho_b} W(\mathbf{r} - \mathbf{r}_b, h) \tag{1}$$

Here, f is the physical quantity, \mathbf{r} is the location vector, m is the mass, ρ is the density, and W is the interpolating kernel function. Parameter h is defined as the smoothing length of the kernel function. The subscript b refers to the quantity evaluated at the position of particle b . Thus, substituting ρ for f , the density at position \mathbf{r} can be written as

$$\rho(\mathbf{r}) = \sum_b m_b W(\mathbf{r} - \mathbf{r}_b, h) . \tag{2}$$

This equation satisfies the continuity equation naturally, because the number and mass of the particles remain constant. As a result, the mass in the computational field is conserved. From eq. (2), the density at the position of particle a can be written as

$$\rho_a = \sum_b m_b W_{ab} , \tag{3}$$

where ρ_a is $\rho(\mathbf{r}_a)$ and W_{ab} is $W(\mathbf{r}_a - \mathbf{r}_b, h)$.

2.2 Momentum equation

The momentum equation is derived from the Navier-Stokes equation as follows [1, 2, 6, 7]:

$$\frac{\partial \mathbf{u}_a}{\partial t} = -\sum_b m_b \left(\frac{p_a}{\rho_a^2} + \frac{p_b}{\rho_b^2} \right) \nabla_a W_{ab} + \sum_b \frac{m_b (\mu_a + \mu_b) \mathbf{u}_{ab}}{\rho_a \rho_b} \left(\frac{1}{r_{ab}} \frac{\partial W_{ab}}{\partial r_a} \right) + \frac{\mathbf{F}_a}{\rho_a}, \quad (4)$$

where \mathbf{u} is the velocity, t is the time, p is the pressure, μ is the viscosity, \mathbf{u}_{ab} is the relative velocity, r_{ab} is the relative distance between particle a and particle b , and \mathbf{F}_a is the body force per unit mass acting on particle a . Since the kernel is symmetric (as mentioned in Section 2.4), it takes the form of

$$\nabla_a W_{ab} = \frac{\mathbf{r}_{ab}}{r_{ab}} \frac{\partial W_{ab}}{\partial r_a}. \quad (5)$$

In the right-hand side of eq. (4), the first term denotes the pressure gradient, and the second term denotes the viscous diffusion.

In the SPH method, because pressure p is obtained by the parameterized density ρ , an incompressible fluid is treated as a quasi-compressible fluid. Therefore, the pressure is obtained from the equation of state for compressible fluid:

$$c = \sqrt{\frac{dp}{d\rho}}, \quad (6)$$

where c is the speed of sound.

2.3 Thermal conduction, salinity diffusion, and buoyancy

Thermal conduction and salinity diffusion are diffusion phenomena. The standard differential equation for thermal conduction or salinity diffusion is written as

$$\frac{\partial f}{\partial t} = \kappa_{T,S} \nabla^2 f, \quad (7)$$

where f represents temperature T or salinity S , κ_T is thermal diffusivity, and κ_S is salinity diffusivity. This equation can be expressed by taking a Taylor expansion of particle a and employing the gradient of the kernel [6, 7]:

$$\frac{\partial f_a}{\partial t} = \sum_b \frac{m_b \kappa_{T,S} (\rho_a + \rho_b) (f_a - f_b) \mathbf{r}_{ab} \cdot \nabla_a W_{ab}}{\rho_a \rho_b r_{ab}^2}. \quad (8)$$

The density of each fluid particle changes, depending on temperature and salinity; however, the effect can be neglected, due to the small thermal expansion coefficient and small salinity diffusivity. Therefore, the density change does not affect the momentum equation (4). By Boussinesq approximation, buoyancy is expressed as

$$F_{B_a} = \frac{\bar{\rho} - \rho'_a(T_a, S_a)}{\bar{\rho}} g, \quad (9)$$

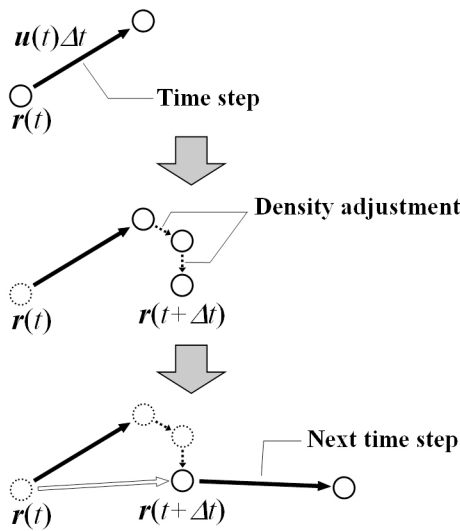


Figure 1. Density adjustment process

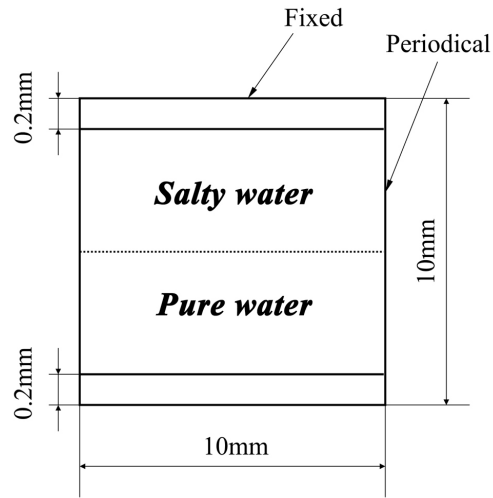


Figure 2. Computational domain for salt-finger simulation

where F_B is buoyancy; ρ'_a is the density of particle a ; $\bar{\rho}$ is the standard density, which is obtained as the average density at the height of the particle; and g is the gravity acceleration. This buoyancy is given as the body force in eq. (4).

2.4 Kernel function

Spline-based interpolated kernels that reduce computational costs are often used, since a potentially small number of neighboring particles are the only contributors in the summations over the particles. In this study, the cubic-spline interpolated kernel called M4-spline function was adopted [25]:

$$W(\mathbf{r}, h) = \frac{\sigma^*}{h^d} \begin{cases} 1 - \frac{3}{2}q^2 + \frac{3}{4}q^3 & \text{if } (0 \leq q < 1) \\ \frac{1}{4}(2-q)^3 & \text{if } (1 \leq q < 2) \\ 0 & \text{if } (2 \leq q) \end{cases} \quad (10)$$

$$\sigma^* = \begin{cases} \frac{2}{3} & : (1 - \text{dimension}) \\ \frac{10}{7\pi} & : (2 - \text{dimension}) \\ \frac{1}{\pi} & : (3 - \text{dimension}) \end{cases}, \quad (11)$$

where d is the number of the dimension, and $q = r/h$ and σ^* are normalized values. With the M4-spline, the quantities of the particles are summed up in the region of $q < 2$.

2.5 Algorithm of Incompressibility

In typical applications (e.g., astrophysics), the SPH method has been used to model compressible flows with high Reynolds numbers. In recent years, the SPH method has also been applied to incompressible flows with low Reynolds numbers. Okachi et al. [8] used a unique algorithm to

simulate Stokes layer and Poiseuille flow. This algorithm has been described as the scheme of the density adjustment process (Fig. 1). In this model, every particle of the fluid first moves according to its own velocity vector. As a result, the density field in the flow becomes non-uniform after one time step. Next, the position of the particle is adjusted based on the pressure gradient due to the density gradient, in order to even out the density non-uniformity. This adjustment continues until the density field becomes uniform, resulting in incompressibility. After this density adjustment process, the velocity vector in the next time step is determined by

$$\mathbf{u}(t + \Delta t) = \frac{\mathbf{r}(t + \Delta t) - \mathbf{r}(t)}{\Delta t}, \quad (12)$$

where Δt is the time difference. Therefore, the particle momentum does not change, and no inertial force is generated during the density adjustment.

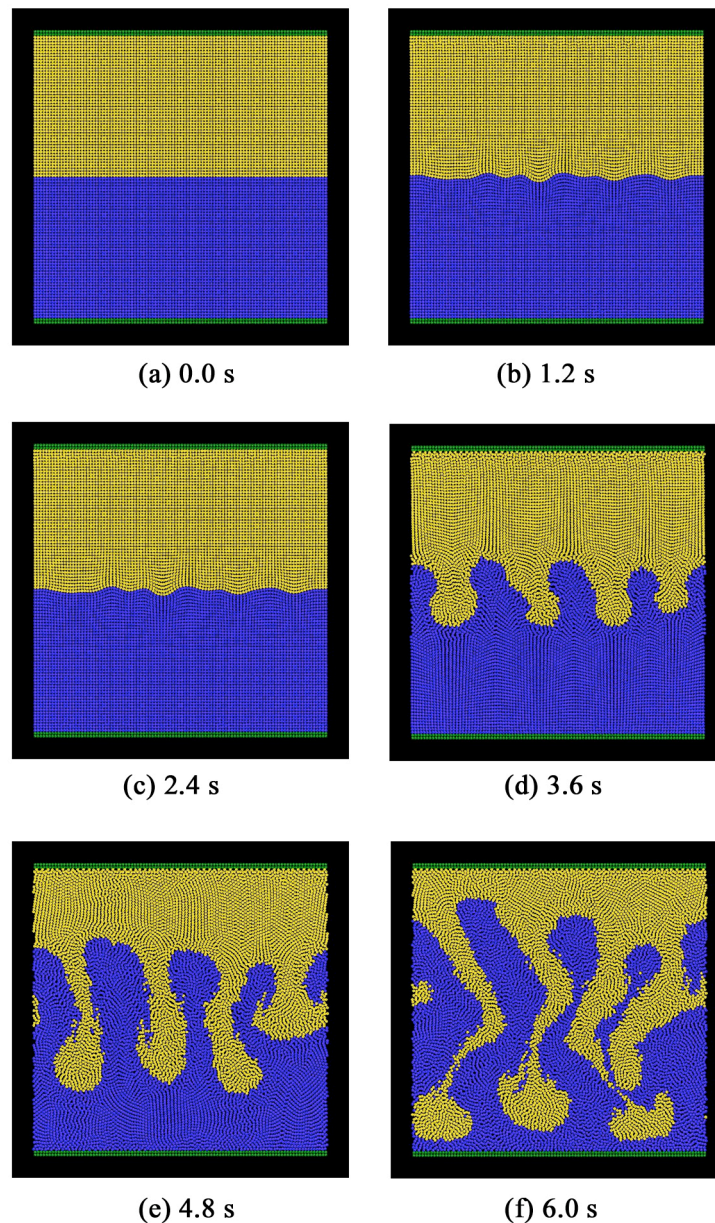


Figure 3. Two-dimensional flow structure of salt fingers

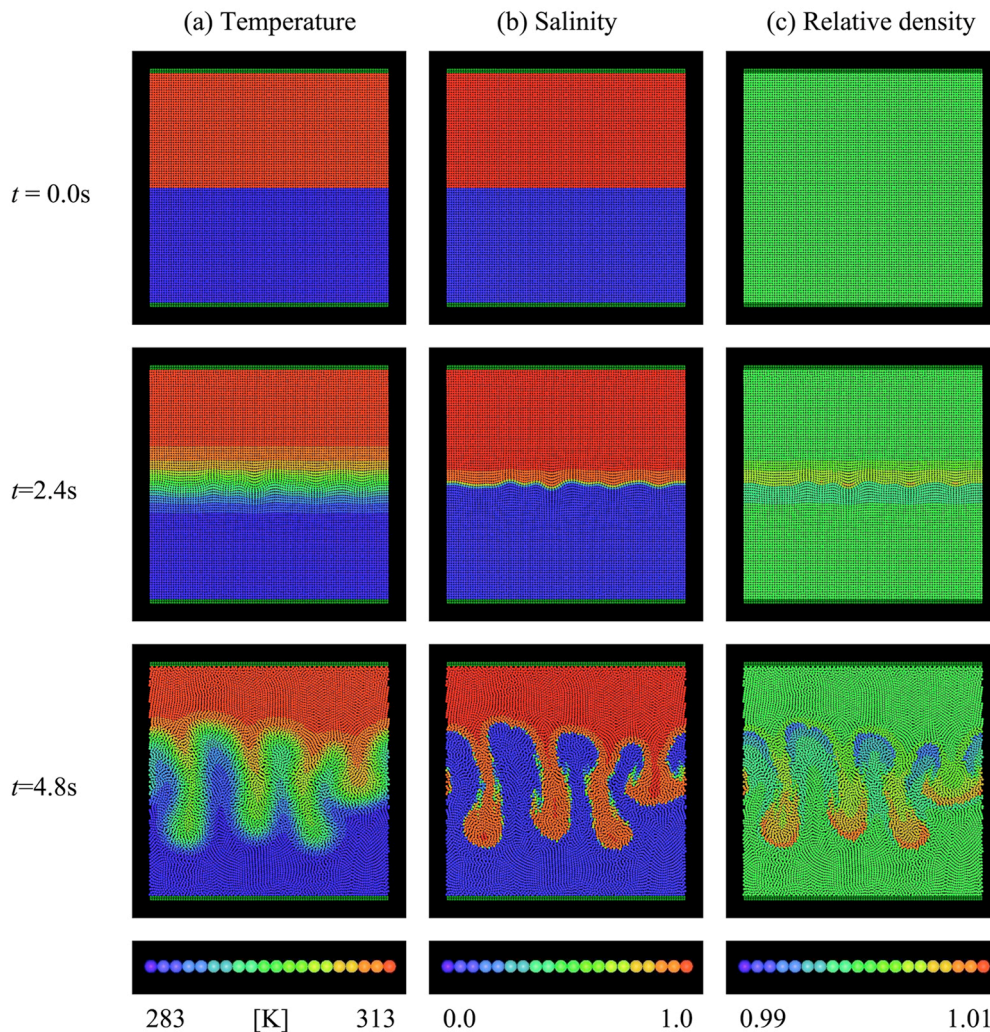


Figure 4. Time evolutions: (a) Temperature, (b) Salinity, (c) Relative density

3. SIMULATION OF THE SALT-FINGER PHENOMENON

3.1 Base case

Figure 2 presents the two-dimensional computational domain for the base case. Its height and width were 10mm each. The diameter of each particle was 0.1mm, and there was a total of 10,000 particles. A periodic boundary condition was imposed on the horizontal direction. The top and bottom walls consisted of two layers of particles whose positions were fixed. Their temperatures were kept constant at 313K and 283K. The upper region was filled with salty water at $T=313\text{K}$ and $S=1.0\%$, and the lower region was filled with pure water at $T=283\text{K}$ and $S=0.0\%$. The Prandtl number varied from 4.3 to 9.5. The ratio of their diffusivities was first set to $\kappa_s/\kappa_T=0.01$.

Figure 3 illustrates the flow structure of the numerical result. The blue particles represent the pure water, the yellow particles represent the salty water, and the green particles denote the wall. With the evolution of time, the interface between the two fluids gradually became wavy and eventually formed several long, slender cells. This is a typical salt-finger phenomenon.

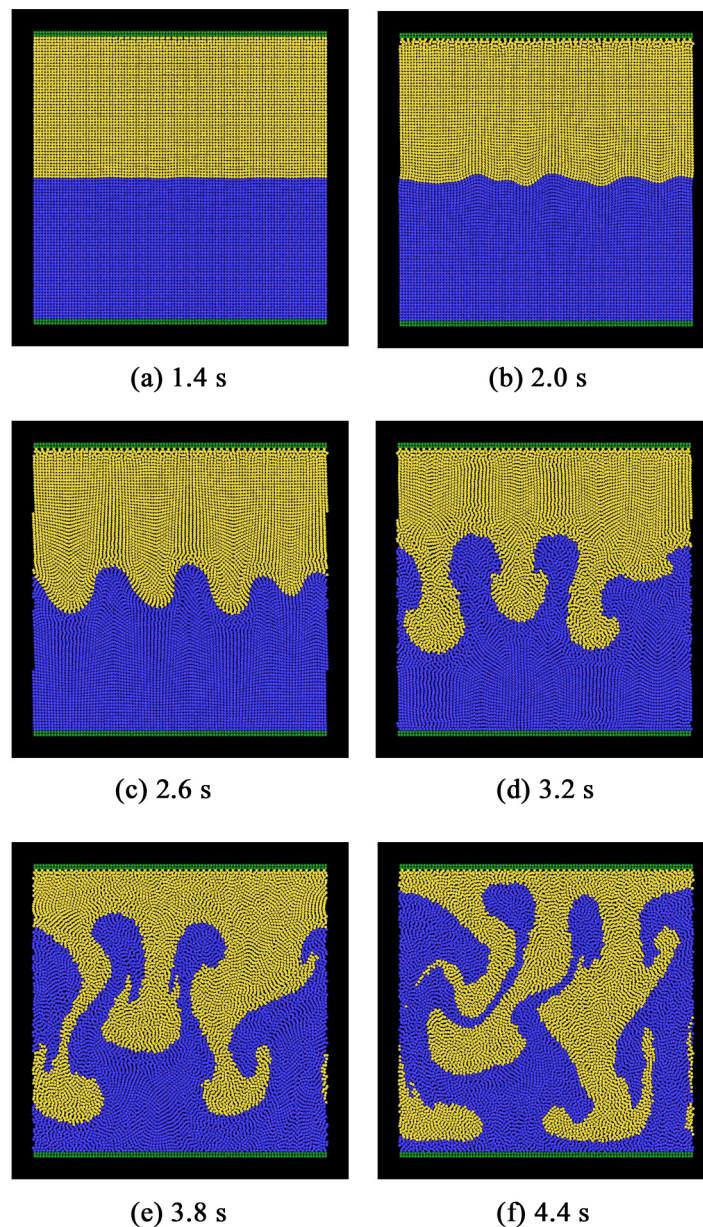
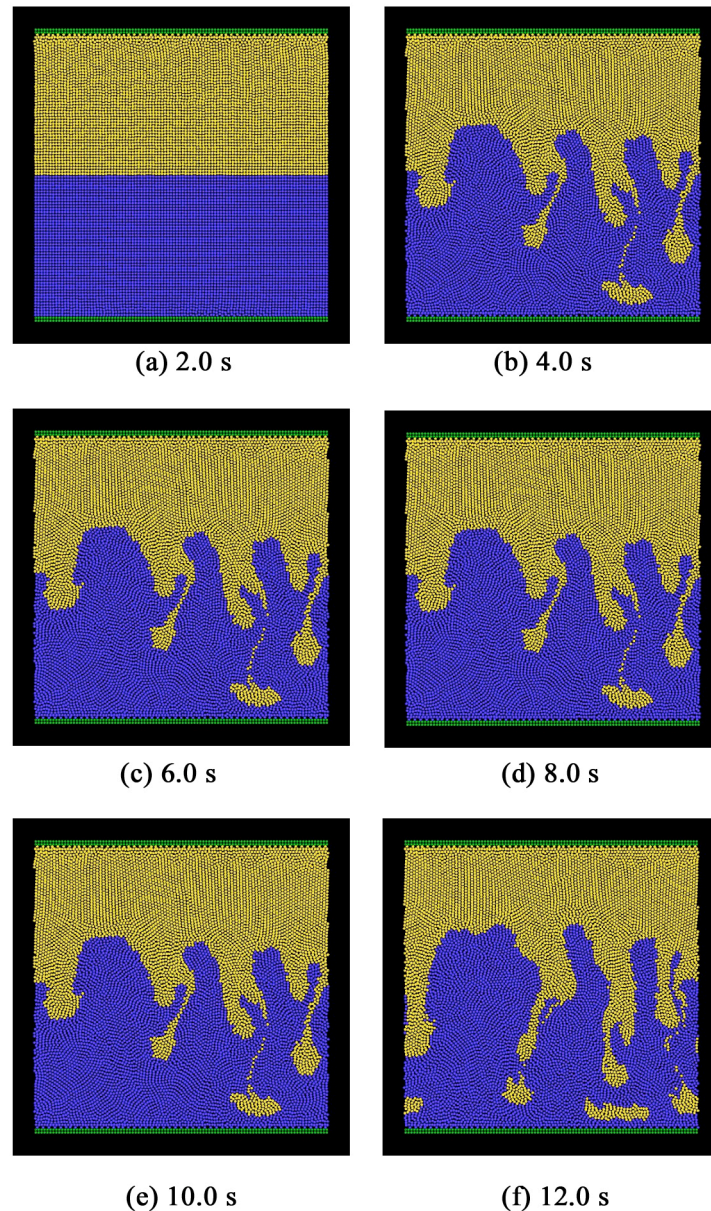


Figure 5. Two-dimensional flow structure of salt fingers ($\kappa_S/\kappa_T=0.001$)

Figure 4 presents the time evolutions of the temperature, the salinity, and the relative density. The temperature diffused through the interface more quickly than the salinity. The temperature diffused before the interface became wavy, while the salinity had hardly diffused at this stage. This produced a density difference, indicating the generation of buoyancy. The temperature changed quickly, and the density progressively decreased at the rising fingers, whereas it progressively increased at the sinking fingers. The isolated small regions of low- or high-density fluids continued to move upward through the field at the tips of the rising fingers, or downward at the tips of the sinking fingers. Therefore, once the salt fingers appeared, they continued to grow, basically because the temperature gradient was large at the fingers. Using a two-dimensional finite-difference scheme, Komurasaki et al. [22] observed a similar flow structure.

3.2 Effect of thermal diffusivity ratio

Figure 6. Two-dimensional flow structure of salt fingers ($\kappa_S/\kappa_T=0.1$)

Fluid motions under different thermal diffusivity ratios were investigated. Figures 5 and 6 depict the time evolutions of flow structures with $\kappa_S/\kappa_T=0.001$ and $\kappa_S/\kappa_T=0.1$. For $\kappa_S/\kappa_T=0.001$, the salt fingers were quickly generated and a drastic convection occurred. Therefore, even after the advancement of temperature diffusion, the initial salinity gradient remained as a dominant driving force, due to the negligibly small effect of the salinity diffusion. However, for $\kappa_S/\kappa_T=0.1$, many thin salt fingers were slowly generated (Fig. 6). Therefore, under this condition, salinity diffusion rather than temperature diffusion was the dominant factor.

Figure 7 (a) reveals the time evolutions of the maximum and the minimum values of the relative densities in the whole computational domain. The maximum values appeared at the front edges of the sinking finger, and the minimum values appeared at the front edges of the rising finger (Figs. 7(b) and (c)). Because the density was discontinuous at the interface, it slightly increased at the first stage of the computation. When the fingers appeared at $t=2\sim 5$ s, the density

changed drastically, and was especially remarkable for $\kappa_S/\kappa_T=0.001$. The rate of this density change was $0.2\% \text{ s}^{-1}$, demonstrating that the present SPH method was capable of simulating the flow with such a high rate of density change. At $t=5\text{s}$, the salt fingers reached the wall, and the density remained constant afterwards. However, for $\kappa_S/\kappa_T=0.1$, the density continued to change gradually, because the salt-finger phenomenon progressed much more slowly than for $\kappa_S/\kappa_T=0.001$. These results confirmed that the present SPH method is a robust and useful scheme, even when the flow conditions changed considerably.

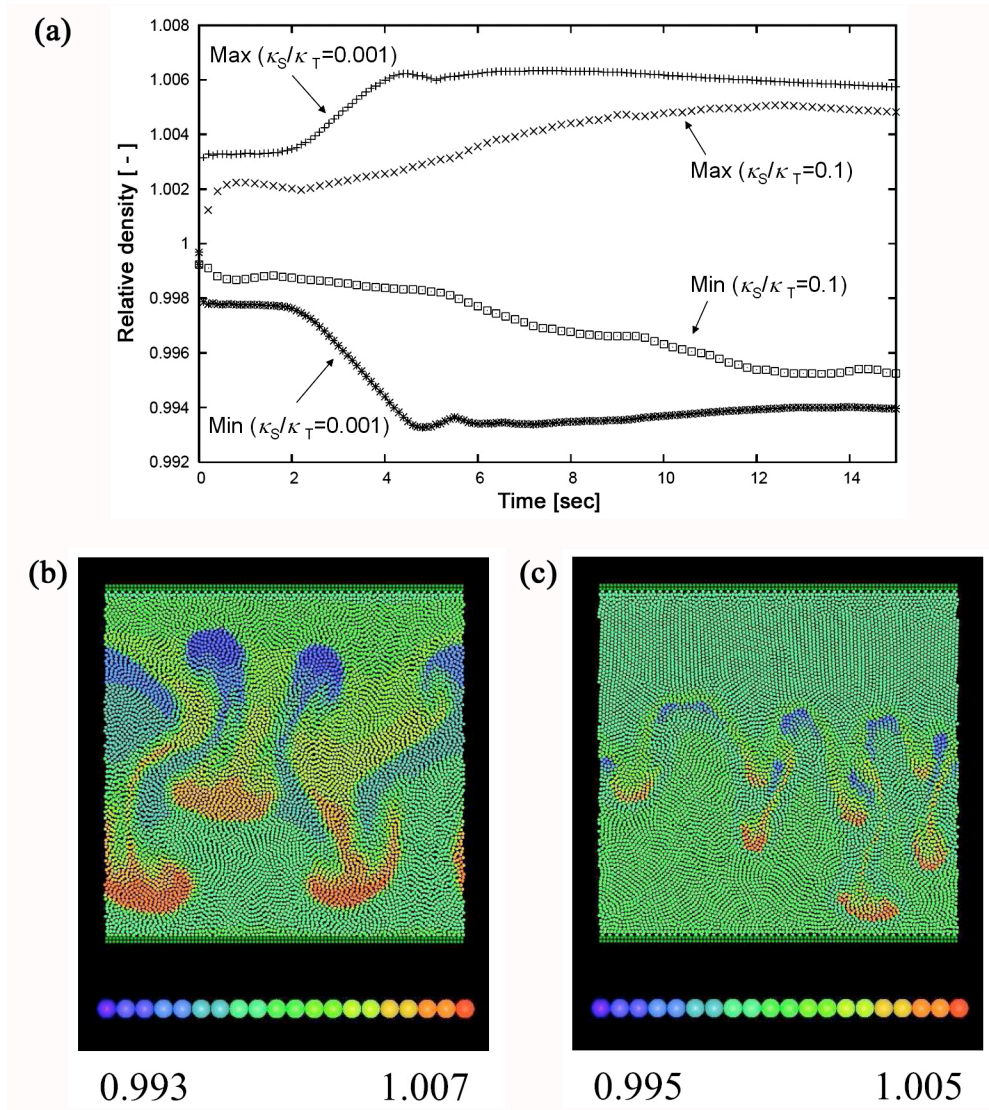


Figure 7. Relative density: (a) Time evolutions of the maximum and minimum values, (b) 2D distribution at $t=5.0\text{s}$ in $\kappa_S/\kappa_T = 0.001$, (c) 2D distribution at $t=8.0\text{s}$ in $\kappa_S/\kappa_T = 0.1$

3.3 Effect of initial density distribution

An incompressible SPH simulation was demonstrated under the condition that the initial distribution of the relative density had a constant gradient in the vertical direction. This distribution was formed from the linear distributions of both temperature and salinity (Fig. 8). Unlike the previous cases, no clear interface existed. The computational domain was set to be 20mm high and 20mm wide. The diameter of each particle was 0.2mm.

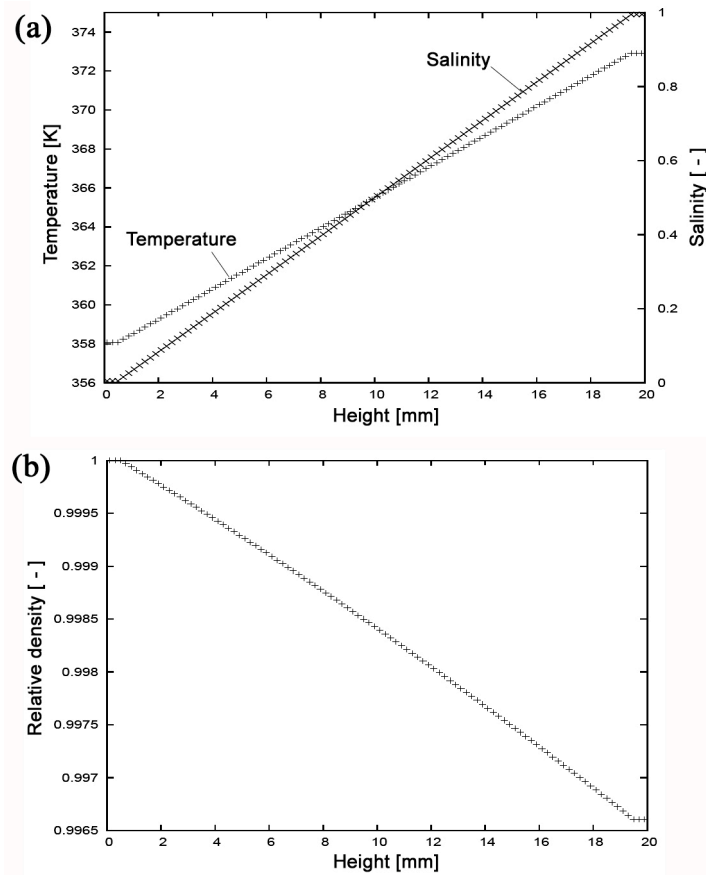


Figure 8. Initial distributions: (a) Temperature and salinity, (b) Relative density

Figure 9 depicts the time evolution of the flow structure. In this figure, the particles are colored blue and yellow merely for the purpose of flow pattern observation. Finger-type convections took place in the whole region. Özgökmen et al. [20] used a two-dimensional finite-difference scheme to compute the salt-finger phenomenon under similar initial conditions. Their result also revealed a flow structure that had finger-type convections in the entire computational region. No discrepancy existed between their numerical results and ours, thus supporting their claim that salt-finger convection can occur not only at the interfaces of discontinuous density but also at fields with a constant density gradient.

3.4 Three-dimensional simulation

The salt-finger phenomenon was simulated by the three-dimensional SPH method. The computational domain was a cube 10mm x 10mm x 10mm. The particle size was 0.1mm, and there was a total of 1,000,000 particles. The other parameters were the same as the base case.

Figure 10 presents the time evolution of the flow field. In this figure, the upper part is depicted on the right-hand side, and the lower part, on the left-hand side. Numerous finger cells were generated and grew. Generations of salt fingers could also be confirmed by three-dimensional numerical simulation. It should be noted that no regularity was observed in the pattern of the generated salt fingers.

Figure 11 reveals the time evolution of the length of one salt finger chosen as an example. At the early stage, the salt finger did not grow. However, it began to grow linearly at $t=2.4s$, where the growth rate was $1.9mm s^{-1}$. After $t=5.0s$, its growth stopped because the salt finger had reached the wall. Taylor et al. [15] experimentally studied the salt-finger phenomenon with a low stability ratio defined as

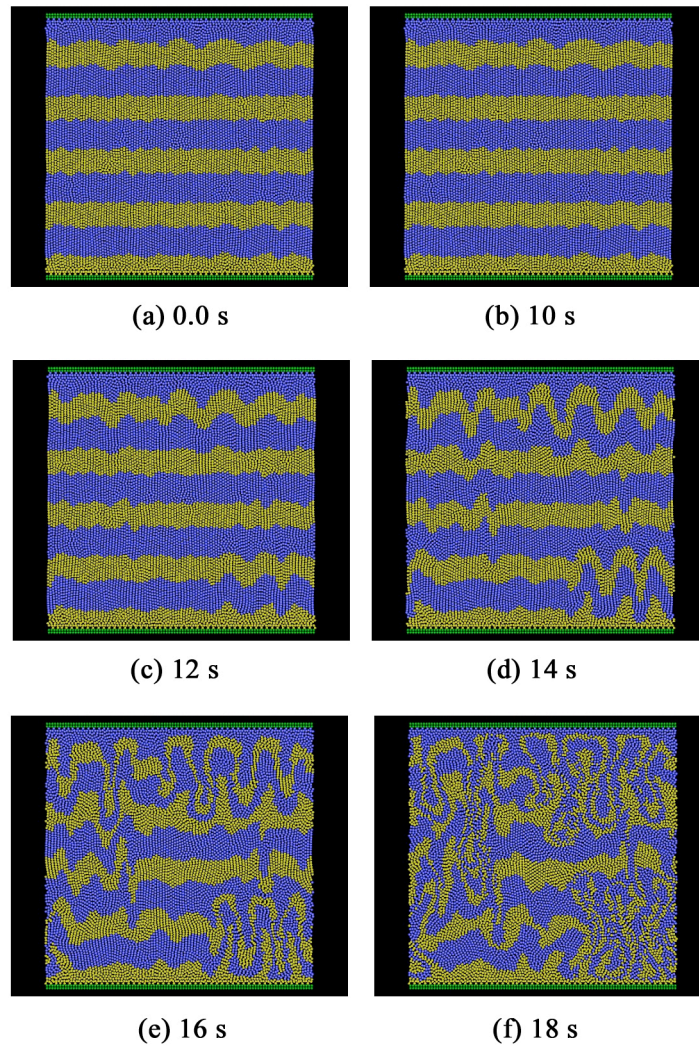


Figure 9. Two-dimensional flow structure of salt fingers (Constant density gradient)

$$R_{\rho} = \frac{\rho_0 \alpha \Delta T}{\rho_0 \beta \Delta S}, \quad (13)$$

where $\rho_0 \alpha \Delta T$ is the stabilizing increment of density due to temperature and $\rho_0 \beta \Delta S$ is the destabilizing increment due to salinity [15]. Their observation of the salt fingers' linear growth agreed with our simulation, although their growth rate was much smaller at $5.7 \times 10^{-3} \text{ mm s}^{-1}$. Thus, it was demonstrated that the SPH was capable of reproducing the basic features of the phenomenon, although a discrepancy in the growth rates remained.

4. SIMULATION OF CHRISTMAS-TREE PHENOMENON

4.1 Two-dimensional simulation

Figure 12 presents the computational domain; the height was 84mm, and the width was 124mm. The diameter of fluid particles was set to 1.0mm. The surrounding walls consisted of two layers of particles, and their positions were fixed. The inside of the wall was filled with water of $T=303\text{K}$. A point source of heat was located 10mm from the lower wall, and had a height of 1.0mm and a width of 1.0mm. Its temperature was fixed to be 353K. The relative density gradient $(1/\rho_0)(d\rho/dy)$ provided by salinity was $7.5 \times 10^{-4} \text{ cm}^{-1}$.

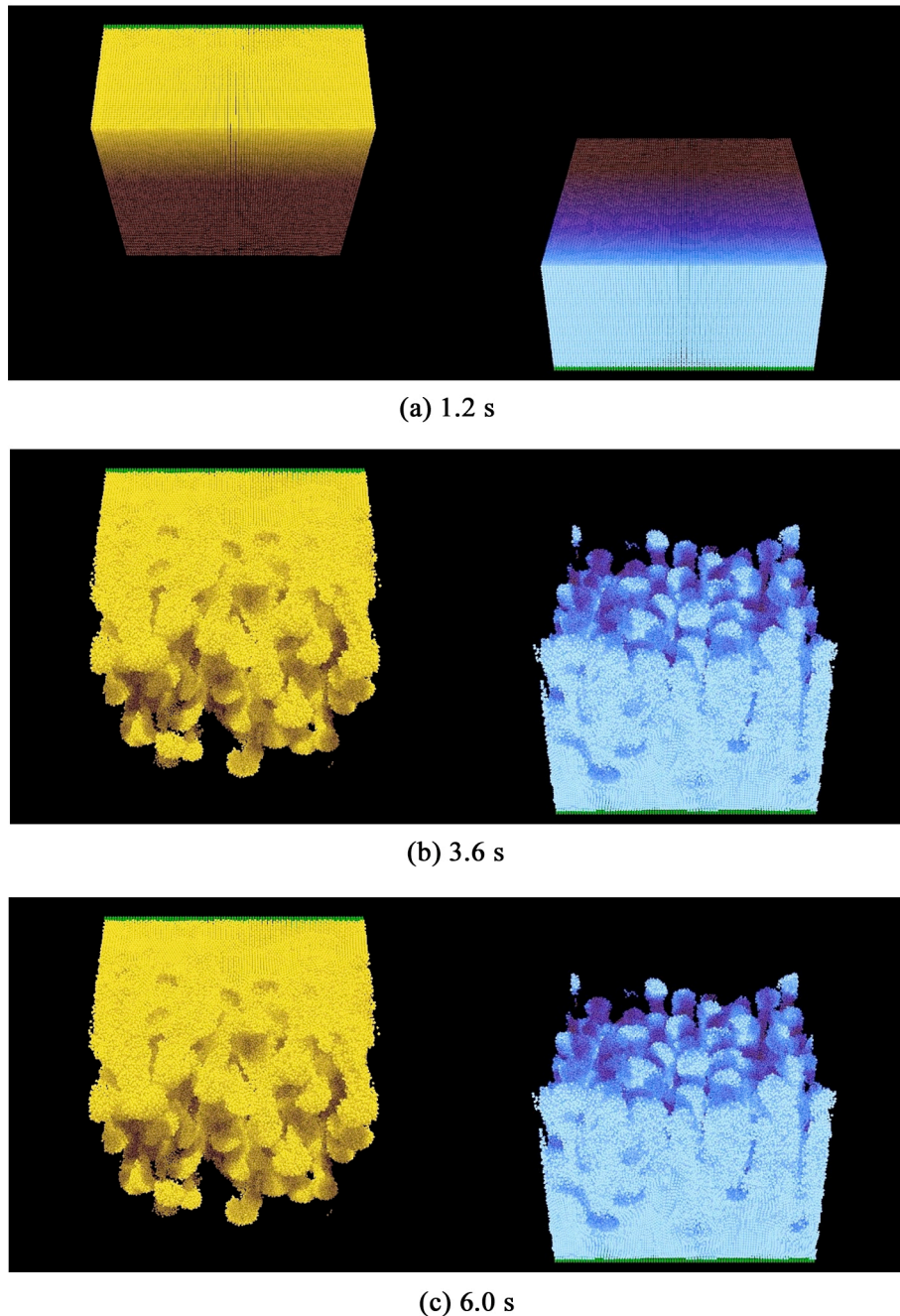


Figure 10. Three-dimensional flow structure of salt fingers

Two cases were computed. In Case 1, a constant density gradient was initially given. In Case 2, however, the initial density had a staircase-like profile with six steps. The initial density profiles of these two cases are plotted in Fig. 13. In the initial stage, the density profile matched the salinity profile because the temperature was the same throughout the fluid.

Figure 14 presents the time evolution of fluid particles in Case 1. The blue and white particles represent water. The white ones are the particles that existed near the vertical centerline in the initial stage of computation. The red particles represent the point source of heat, and the green ones denote the walls. In Case 1, a plume was generated at the point source of heat and spread horizontally by thermal convection. An indication of the generation of a second plume was observed, but it was not clear.

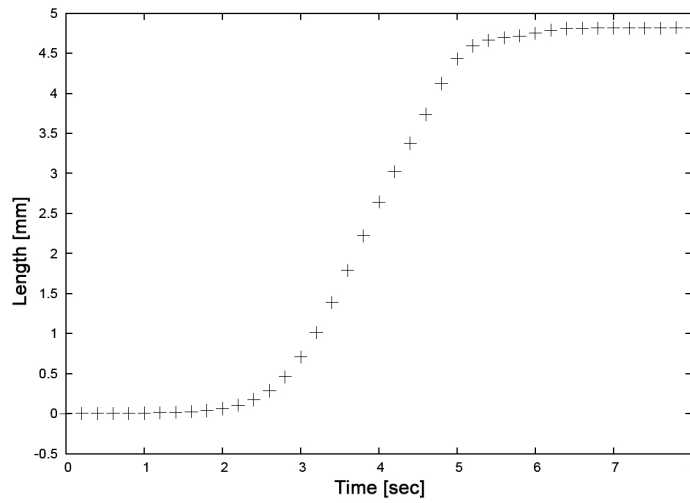


Figure 11. Growth of a salt finger

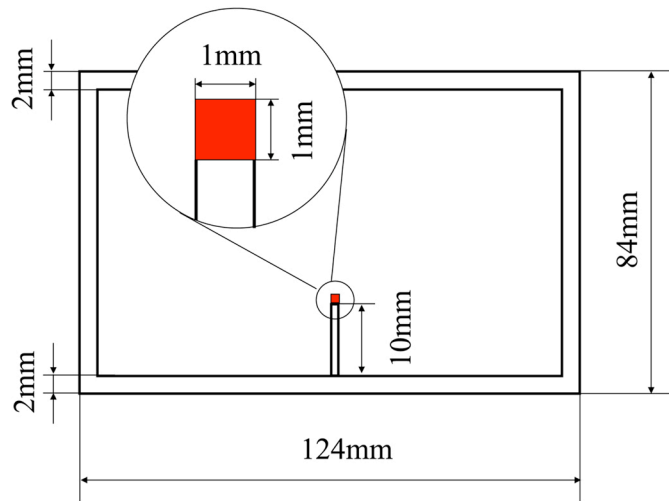


Figure 12. Computational domain for Christmas-tree simulation

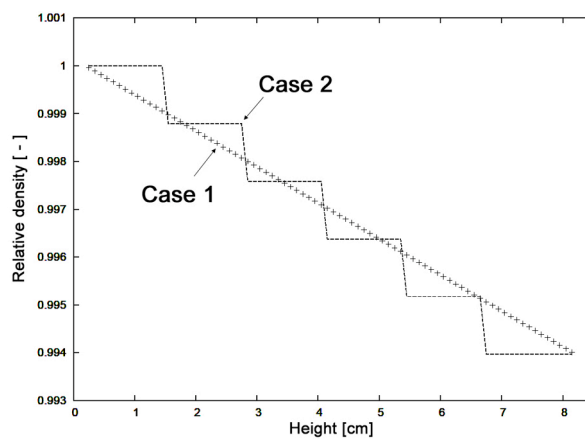


Figure 13. Initial distributions of relative density

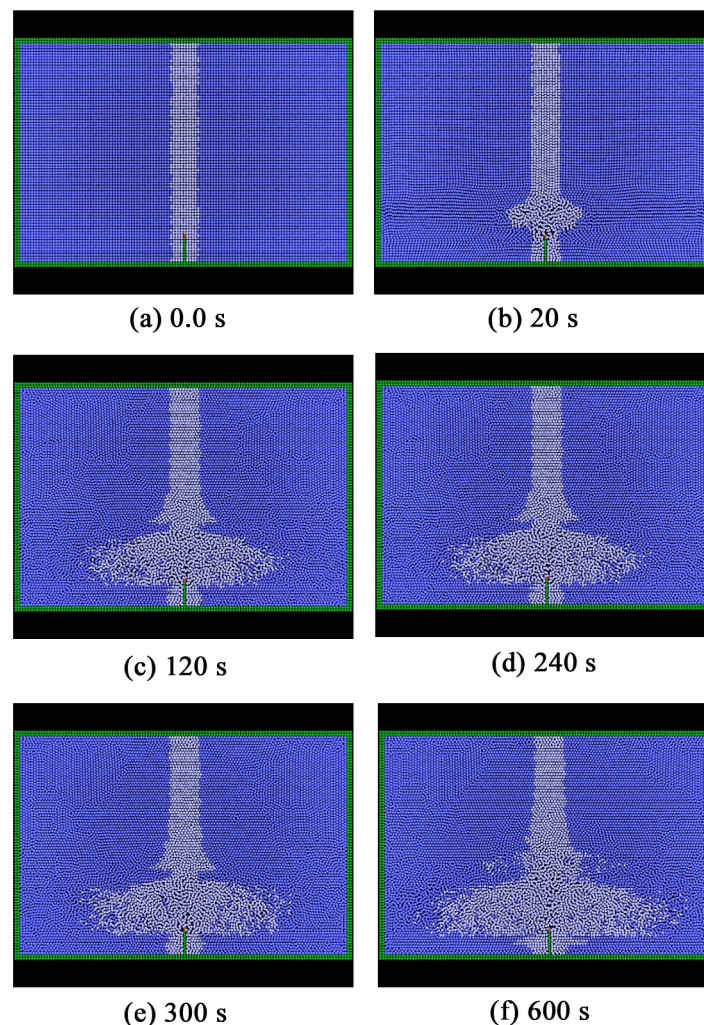


Figure 14. Two-dimensional flow structure in Case1

In Case 2, the Christmas-tree convection was clearly observed (Fig. 15). Horizontal branches were formed along with the six layers of the steps of salinity. The first horizontal convection layer was generated on the lowest layer of salinity. Subsequently, the following horizontal layers appeared one after another as time evolved. It was assumed that the small density jumps in the original salinity profile triggered this phenomenon.

The report by Tsinober et al. [23] did not clearly state how the salinity gradient was created in their experiment. However, in these kinds of experiments, the tank is usually filled with the heaviest liquid at the bottom, and then slightly lighter liquid is gradually piled on top. The density profile thus exhibits a staircase form, which will hopefully smooth out by molecular diffusion with sufficient time. Thus, it is possible that the original staircase-like profile remained while the experiment was carried out, as the present result of the numerical simulation suggested.

4.2 Three-dimensional simulation

Three-dimensional simulation was conducted under the same conditions as in Case 2. In the three-dimensional simulation, the computational domain was a cylinder with a diameter of 126mm and a height of 86mm. There was a total of 1,057,972 fluid particles. The other parameters were the same as indicated in the previous section.

The results are presented in Figs. 16 and 17. The staircase-like density profile, corresponding with the salinity profile, had six steps. The computational domain was filled with fluid particles of water. In Fig. 16, the blue, yellow and pink particles represent the water particles. The blue and

yellow particles are colored merely for observation purposes. The pink particles in Fig. 16 and the white ones in Fig. 17 represent the water particles that existed near the vertical centerline in the initial stage of the computation. The green and black particles represent the top/bottom walls and the side wall. A part of the wall is cut out in both figures. The “Christmas tree” formation can be observed in the computation, revealing results that were similar to those of the two-dimensional computation in Fig. 15.

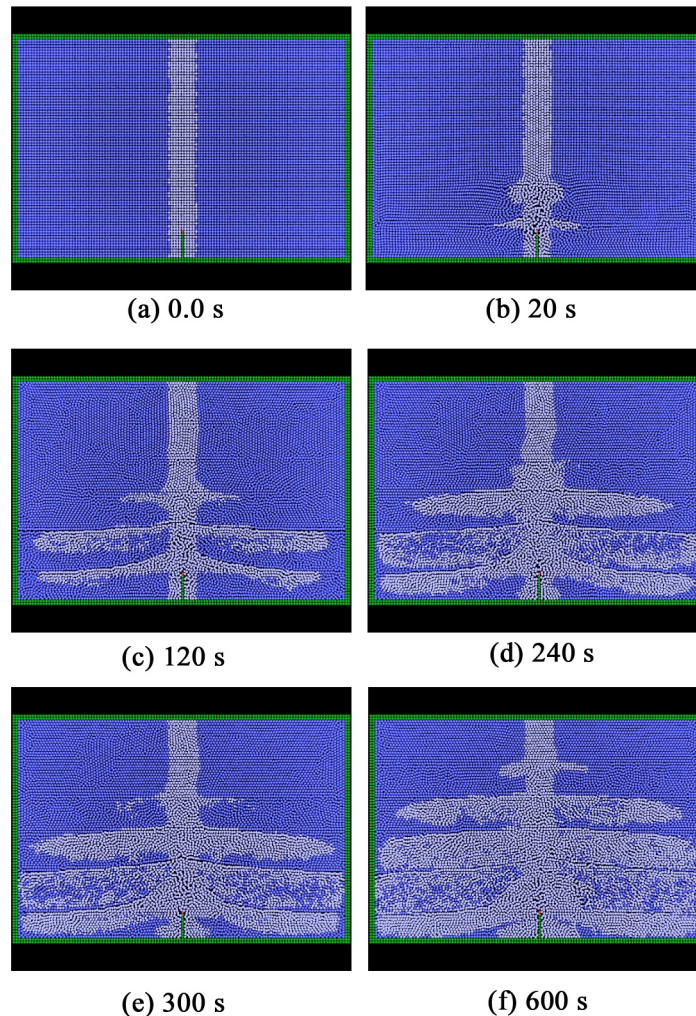


Figure 15. Two-dimensional flow structure in Case2

Figure 18 presents the time evolution of the laterally spreading area of the three layers. The first layer appeared, and then the second layer was immediately generated above the first one. Both layers spread with similar speed. Subsequently, the third layer started to grow at $t=100$ s. Tsinober et al. [23] reported that the convection layers spread in proportion to time progression. Our present computation also exhibited the same tendency. Therefore, it was concluded that the present three-dimensional computational result by the incompressible SPH method was in good qualitative agreement with the experiment results [23]. However, Tsinober et al. [23] reported much smaller growth rates of the layers than in our computation. This discrepancy was probably due to the limited space-resolution in our computation and the fact that the tank diameter had to be much smaller in our computation than in their experiment, due to limitations of computational resources. Meanwhile, the outward flow of the spreading layer induced a reverse flow below the layer, to satisfy continuity (Fig. 16). The effect became larger, especially when the tank radius was small, and the induced reverse flow affected the growth of the layer.

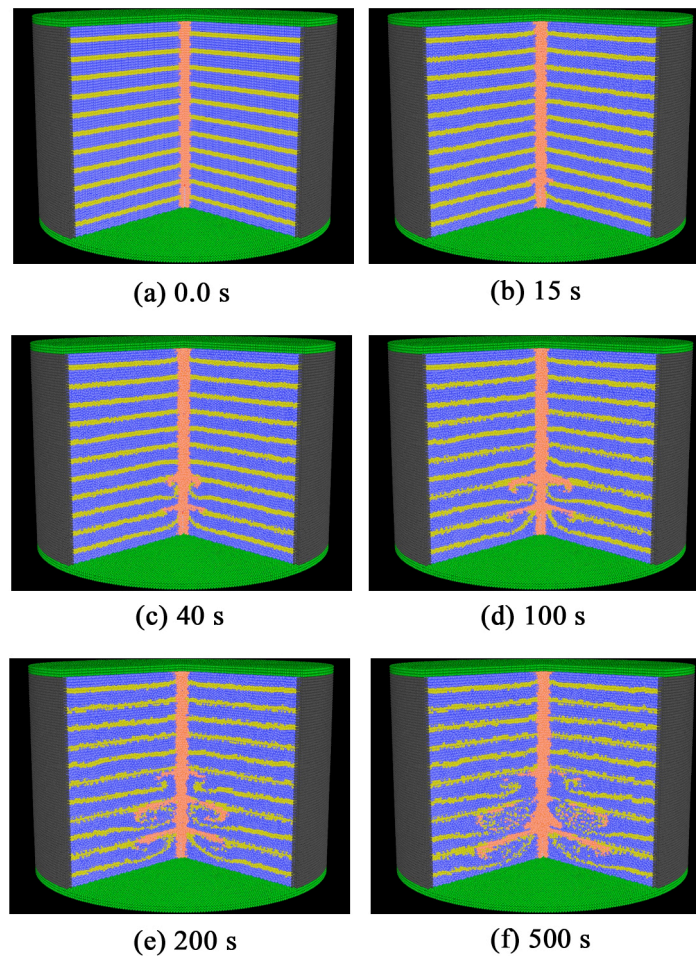


Figure 16. Three-dimensional flow structure of Christmas tree phenomenon in Case2

5. CONCLUSION

An incompressible SPH method was developed to simulate double-diffusive convection phenomena, including the simultaneous diffusion of temperature and salinity, and both two- and three-dimensional simulations were successfully carried out. In particular, it was demonstrated that the newly developed computational scheme was capable of simulating the instability at the interface between liquids with two different densities, and the salt-finger phenomenon could be clearly observed in the results. The results also indicated that the ratio between the speed of temperature conduction and salinity diffusion controlled the overall phenomenon.

The so-called “Christmas-tree phenomenon” was also simulated. The results revealed that this phenomenon did not take place when the salinity profile had a vertically constant gradient, but only when the original salinity profile had a staircase-like profile with layers of several steps.

The present computation for double-diffusive convection problems exhibited qualitatively good results, indicating that this newly developed SPH method may be applicable to the simulation of phenomena caused by a small change in density. However, it is necessary to examine the accuracy of this technique quantitatively by comparison with experimental results that are often very difficult to obtain. The lack of good quantitative experimental data is always a major problem; however, despite the challenges, carrying out the experiments will be essential to developing trustworthy computational methods.

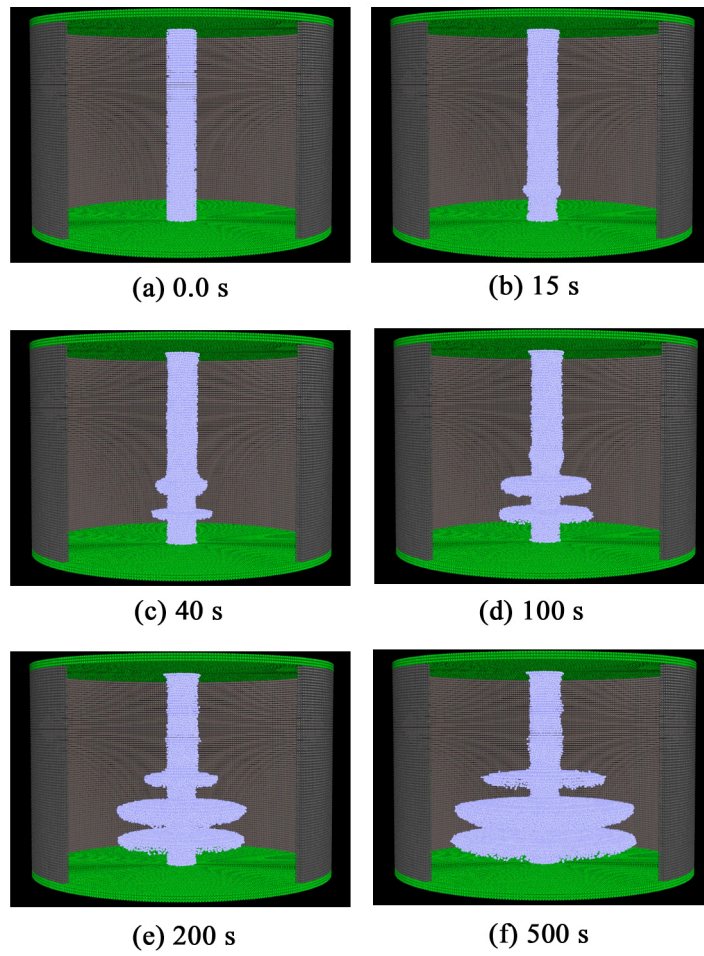


Figure 17. Three-dimensional flow structure of Christmas tree phenomenon in Case2

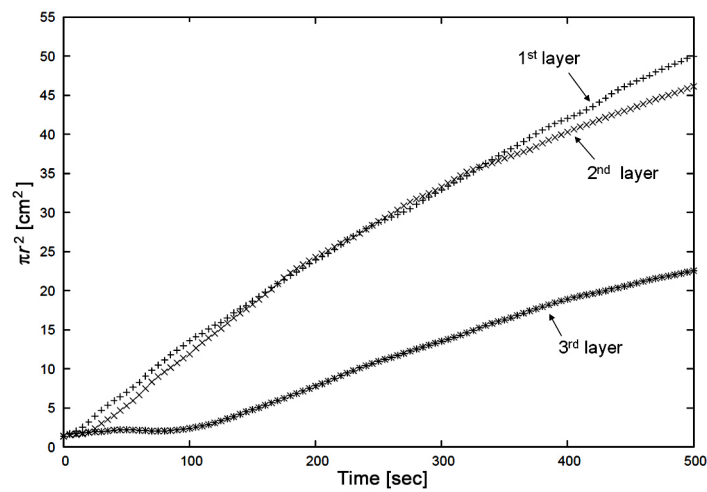


Figure 18. Time evolution of layer area πr^2 (r is the layer radius)

ACKNOWLEDGEMENTS

The authors express their sincere thanks to Dr. Tetuya Kawamura and Dr. Satoko Komurasaki for valuable and meaningful discussions.

REFERENCES

- [1] L.B. Lucy, A Numerical Approach to the Testing of the Fission Hypothesis, *The Astronomical Journal*, 82, 1977, 1013-1024.
- [2] R.A. Gingold and J.J. Monaghan, Smoothed Particle Hydrodynamics: Theory and Application to Non-spherical Stars, *The Astronomical Journal*, 181, 1977, 375-389.
- [3] L.D. Libersky, A.G. Petschek, T.C. Carney, J.R. Hipp, and F.A. Allahdadi, High Strain Lagrangian Hydrodynamics, *Journal of Computational Physics*, 109, 1993, 67-75.
- [4] P.W. Cleary and J.J. Monaghan, Conduction Modeling Using Smoothed Particle Hydrodynamics, *Journal of Computational Physics*, 148, 1999, 227-264.
- [5] J.J. Monaghan, Simulating Free Surface Flows with SPH, *Journal of Computational Physics*, 110, 1994, 399-406.
- [6] J.P. Morris, P.J. Fox, and Y. Zhu, Modeling Low Reynolds Number Incompressible Flows Using SPH, *Journal of Computational Physics*, 136, 1995, 214-226.
- [7] J.J. Monaghan, Heat Conduction With Discontinuous Conductivity, *Applied Mathematics Reports and Preprints*, Monash University (1995).
- [8] N. Okachi, A. Hirota, S. Izawa, Y. Fukunishi, and H. Higuchi, SPH Simulation of Pulsating Pipe Flow at a Junction, *Proceedings of 1st International Symposium on Advanced Fluid Information*, 2001, 388-391.
- [9] T. Nemoto, S. Izawa, A.X. Xiong, and Y. Fukunishi, SPH Method Simulation of the Flow with Heat Convection, *Proceedings of JSME Tohoku Section Honjyo Conference*, 041(2), 2004, 85-86. (in Japanese)
- [10] T. Sano, S. Izawa, A.X. Xiong, and Y. Fukunishi, The Numerical Simulation of Flow which Has Free Surface and Deformation Boundary by SPH Method for Incompressible Fluid, *Proceedings of 83th JSME Fluids Engineering Conference*, 2005, CD-ROM. (in Japanese)
- [11] H. Stommel, A.B. Arons, and D. Blanchard, An oceanographic curiosity: the perpetual salt fountain, *Deep-Sea Research*, 3, 1956, 152-153.
- [12] J.S. Turner and H. Stommel, A new case of convection in the presence of combined vertical salinity and temperature gradients, *Proceeding of National Academy of Science, U. S. A.*, 52, 1964, 49-53.
- [13] J.S. Turner, Salt fingers across a density interface, *Deep-Sea Research*, 14, 1967, 599-611.
- [14] H.E. Huppert and J.S. Turner, Double-diffusive convection, *Journal of Fluid Mechanics*, 106, 1981, 299-329.
- [15] J.R. Taylor and G. Veronis, Experiments on Double-Diffusive Sugar-Salt Fingers at High Stability Ratio, *Journal of Fluid Mechanics*, 321, 1996, 315-333.
- [16] R.W. Schmitt, Observational and laboratory insights into salt-finger convection, *Progress in Oceanography*, 2003, doi:10.1016/S0079-6611(03)00033-8.
- [17] M.E. Stern, The 'salt-fountain' and thermohaline convection, *Tellus*, 12, 1960, 172-175.
- [18] E. Kunze, A review of salt-fingering theory, *Progress in Oceanography*, 2003, doi:10.1016/S0079-6611(03)00027-2.
- [19] S.A. Piacsek and J. Toomre, Nonlinear evolution and structure of salt fingers, *Nihoul, J.C.J. Ed. Marine Turbulence: Proceedings of the 11th International Liège Colloquium on Ocean Hydrodynamics. Elsevier Oceanography Series*, 28, 1980, 193-219.
- [20] T.M. Özgökmen, O.E. Esenkov, and D.B. Olson, A numerical study of layer formation due to fingers in double-diffusive convection in a vertically-bounded domain, *Journal of Marine Research*, 56, 1998, 463-487.
- [21] Y. Suenaga, S. Komurasaki, and T. Kawamura, Thermal Convection in salty stratified fluid, *Proceedings of 2004 Meeting of Japan Society of Fluid Mechanics*, 2004, D233. (in Japanese)
- [22] S. Komurasaki, K. Kuwahara, and T. Kawamura, Simulation of a Double Diffusive Convection for Salt Fingers and Formation of Uniform-Density Layer, *Proceedings of 46th AIAA Aerospace Sciences Meeting and Exhibit*, 2008, 575 (8 pages).
- [23] A.B. Tsinober, A. Yahalom, and D.J. Shlien, A Point Source of Heat In a Stable Salinity Gradient, *Journal of Fluid Mechanics*, 135, 1983, 199-217.
- [24] Y. Suenaga, T. Kawamura, and S. Komurasaki, Numerical study of thermal convection above the point heat source in a salinity gradient, *Abstract book of 57th Annual Meeting of the Division of Fluid Dynamics, American Physical Society*, 2004, #NE.007.
- [25] J.J. Monaghan and J.C. Lattanzio, A Refined Particle Method for Astrophysical Problems, *Astronomy and astrophysics*, 149, 1985, 135-143.